# Electronic structure of the antiferromagnetic semiconductor $MnSb_2S_4$

S. F. Matar*
*Institut de Chimie de la Matière Condensée de Bordeaux CNRS, Université Bordeaux 1, 87 Avenue du Dr. Albert Schweitzer, F-33608 Pessac Cedex, France*

R. Weihrich, D. Kurowski, and A. Pfitzner
*Institut für Anorganische Chemie, Universität Regensburg, Universitätsstrasse 31, D-93040 Regensburg, Germany*

V. Eyert
*Institut für Physik, Universität Augsburg, D–86135 Augsburg, Germany*
(Received 19 January 2005; revised manuscript received 11 April 2005; published 29 June 2005)

The electronic band structures of orthorhombic (*oP28*) and monoclinic (*mC28*) $MnSb_2S_4$ were investigated with *ab initio* calculations in the local spin density approximation to the density functional theory. An analysis of the electronic properties and of the chemical bonding is provided using the augmented spherical wave method considering nonmagnetic, ferromagnetic, ferrimagnetic, and antiferromagnetic model orderings. In agreement with experimental results both modifications of $MnSb_2S_4$ are predicted to be antiferromagnetic. While the experimental band gap is missed for the monoclinic polymorph, the calculated band gap for orthorhombic $MnSb_2S_4$ is close to the experimental one.

DOI: 10.1103/PhysRevB.71.235207 PACS number(s): 71.15.Mb, 62.20.Qp, 71.20.−b, 79.20.Uv

## I. INTRODUCTION

Magnetic and semiconducting manganese sulphides attracted the attention of solid state chemists since the early days of x-ray crystallography and magnetic structure investigations[1–5] done on haurite ($MnS_2$) and alabandite (MnS). They exhibit high magnetic moments due to the coordination of $Mn^{2+}$ in $MnS_6$ octahedra where it prefers a high spin state with five unpaired electrons. However, $MnS_2$ has been discussed as a rare example of a high spin to low spin transition under high pressure.[6,7]

In the past few years the chemistry of magnetic manganese materials was enriched by fascinating discoveries mainly on multinary manganese oxides.[6–8] Properties like the giant and colossal magnetoresistance (GMR, CMR) inspired new fields of research on magnetic semiconductors. Besides promising technological applications and experimental challenges there is an increasing demand and success of theoretical understanding of the underlying chemical bonding and electronic properties. The development and application of effective density functional (DFT) methods within the local spin density approximation (LSDA) still plays an increasing role herein.[9–11]

Fascinating properties were also discovered on manganese chalcogenides. MnS and $MnS_2$ show antiferromagnetic ordering while diluted magnetic semiconductors (DMS) based on MnS exhibit outstanding properties related to spintronic applications.[12–14] Multinary materials like $MnCr_2S_4$ provide additional potential with respect to anisotropic resistivity and magnetic properties.[15,16]

Due to its reduced dimensionality $MnSb_2S_4$ serves as a promising low dimensional magnetic semiconducting material. Contrary to spinel type $MnCr_2S_4$ with $Mn^{2+}$ in $MnS_4$ tetrahedra one finds $MnS_6$ octahedra in $MnSb_2S_4$. Therein, it is related to MnS and $MnS_2$ as well as in the observation of phase transitions. Orthorhombic $MnSb_2S_4$ is accessible by hydrothermal synthesis and was earlier shown[17] to be isotypic to $FeSb_2S_4$ which is an antiferromagnetic material.[18] Recently a new monoclinic modification (*mC28*) of $MnSb_2S_4$ was synthesized by high temperature methods.[19] $MnSb_2S_4$ (*mC28*) can be transformed reversibly into the orthorhombic modification (*oP28*) at high pressure.[20] By electrical conductivity and magnetic susceptibility measurements it was found that $MnSb_2S_4$ (*mC28*) is a semiconducting antiferromagnet with $T_N=26.5$ K and an electronic band gap of 0.77 eV.[19,20] Concerning the bonding situation one faces one-dimensional (1D) magnetic interactions, as well as bonds with and within the $[SbS_3]^{3-}$ ligand network that is related to $Sb_2S_3$.[24] However, no theoretical investigations are reported yet. Considering MnS and $MnS_2$ again as prominent examples, LSDA calculations[21–23] achieved good agreement with experimental results, i.e., the prediction of semiconducting and magnetic ground states with moments around 4.5 $\mu_B$ for $Mn^{2+}$. For $\alpha$-MnS the antiferromagnetic ground state was correctly found.[21,22] LSDA total energy calculations on $MnS_2$ supported the possibility of a low spin/high spin phase transition for a compressed cell.[22]

To discuss the differences and relations of the bonding, spin states and magnetic ordering in *mC28* and *oP28* $MnSb_2S_4$ first principles calculations are subsequently reported modeling nonmagnetic (NM), ferromagnetic (FM), ferrimagnetic (FIM for the monoclinic system), and antiferromagnetic (AFM) structures in order to identify the ground state configuration. The applied augmented spherical wave (ASW) method was successfully used in previous calculations on magnetic semiconducting manganites.[11] The crystal structures, computational details, and results of the calculations on nonmagnetic, ferromagnetic, and antiferromagnetic configurations are presented, as well as electronic band structures, site projected densities of states, and chemical bonding characteristics.

 

TABLE I. Crystal data from literature and calculation results for orthorhombic (*oP28*) and monoclinic (*mC28*) $MnSb_2S_4$, NSP=nonspin polarized; FM=ferromagnetic; FIM=ferrimagnetic; and AFM =antiferromagnetic.

| Parameters (Refs. 19 and 20) | $MnSb_2S_4$ (*oP28*) | $MnSb_2S_4$ (*mC28*) |
|---|---|---|
| Space group | *Pnam* (62) | *C*2/*m* (12) |
| *a b c* (Å) | 11.457 14.351 3.823 | 12.747 3.799 15.106 $\beta$=113.9° |
| $\langle d_{Mn—S}(Å)\rangle$ | 2.588 | 2.611 |
| $\langle d_{Sb—S}(Å)\rangle$ | 2.551 | 2.532 |
| $\Delta E_{FM\text{-}NSP}$(eV/fu) | −1.441 | −1.436 |
| $\Delta E_{FIM\text{-}FM}$(eV/fu) | | −0.0133 |
| $\Delta E_{AFM\text{-}FM}$(eV/fu) | −0.020 | −0.073 |
| $\Delta E_{AFM1\text{-}FM}$(eV/fu) | −0.014 | |
| $M^{FM}_{Mn}$ ($\mu_B$) | 4.384 | 4.138/4.200 |
| $M^{FM}_{S}$ ($\mu_B$) | 0.060/0.110 | 0.059/0.060 |
| $M^{FM}_{Sb}$ ($\mu_B$) | 0.060/0.080 | 0.08/0.13 |
| $M^{FM}_{cell}$ ($\mu_B$) | 20.0 | 9.82 |
| $M^{FIM}_{Mn}$ ($\mu_B$) | | +4.180/−4.11 |
| $M^{FIM}_{S}$ ($\mu_B$) | | +0.049/−0.047 |
| $M^{FIM}_{Sb}$ ($\mu_B$) | | −0.116/+0.095/+0.055/−0.088 |
| $M^{FIM}_{cell}$ ($\mu_B$) | | 0 |
| $M^{AFM1}_{Mn}$ ($\mu_B$) | ±4.341 | ±(4.181/4.121) |
| $M^{AFM1}_{S}$ ($\mu_B$) | ±0.0003/0.0 | ±(0.001/0.09) |
| $M^{AFM1}_{Sb}$ ($\mu_B$) | ±0.056 | ±(0.004/0.052) |
| $M^{spin\uparrow-spin\downarrow}_{cell}$ ($\mu_B$) | ±9.1 | ±8.93 |
| $M^{AFM1}_{cell}$ ($\mu_B$) | 0 | 0 |
| $M^{AFM2}_{Mn}$ ($\mu_B$) | ±4.35 | |
| $M^{AFM2}_{S}$ ($\mu_B$) | ±0.051/0.019 | |
| $M^{AFM2}_{Sb}$ ($\mu_B$) | ±0.092/±0.029 | |
| $M^{spin\uparrow-spin\downarrow}_{cell}$ ($\mu_B$) | ±9.00 | |
| $M^{AFM2}_{cell}$ ($\mu_B$) | 0 | |

## II. CRYSTAL STRUCTURES OF ORTHORHOMBIC AND MONOCLINIC PHASES

For the calculations presented herein, the crystal structures of both $MnSb_2S_4$ modifications as determined by single crystal x-ray diffraction were taken as the starting points.[17,19,20] The space groups and the relevant lattice parameters used in the calculation are given in the first part of Table I. Both modifications are based on chains of edge-sharing $MnS_6$ octahedra (Fig. 1). These chains of octahedra are linked by $[SbS_3]^{3-}$ units to form layers in the case of $MnSb_2S_4$ (*mC28*) and a three-dimensional (3D) network in the case of $MnSb_2S_4$ (*oP28*).

The Sb—S bonds determine both the structural anisotropies and the differences between the modifications. Sb atoms exhibit a $3+2+x$ ($x=1,2$) coordination with three Sb—S bonds of about 2.5 Å and two Sb—S bonds between 2.9 and 3.1 Å ("secondary bonds"). In addition, there are so-called nonbonding distances 3.1 Å $< d$(Sb—S) $<$ 4 Å. Distinguishing these three types of Sb—S interactions we find all short Sb—S bonds linking edge sharing $MnS_6$-octahedra of one chain in $MnSb_2S_4$ (*mC28*). Slightly longer bonds link the octahedra to form a layered structure (Fig. 1). Between the layers (along the *c* axis) only so-called nonbonding Sb—S distances are found. In the case of $MnSb_2S_4$ (*oP28*) one finds double chains of octahedra which are interlinked by short and secondary Sb—S bonds. These double chains form a kind of fishbone scheme and nonbonding Sb—S distances between them result in a 3D network. The density of the title compound increases from 4.24 g/cm$^3$ (*mC28*)[19] to 4.51 g/cm$^3$ (*oP28*),[17] showing that the orthorhombic modification is the high pressure form. The distances $d$(Mn—S) vary from around 2.5 to 2.7 Å (Table I) in both modifications. Thus they show a slightly broader range than in the pure manganese sulphides with octahedral coordination of manganese, i.e., $d$(Mn—S)=2.61 Å in $\alpha$-MnS[2] and $d$(Mn—S)=2.59 Å in $MnS_2$.[1] There are two different Mn positions in $MnSb_2S_4$ (*mC28*), with a higher site symmetry than the single Mn position in $MnSb_2S_4$ (*oP28*). The distortions of the $MnS_6$ octahedra are due to the structural aniso-

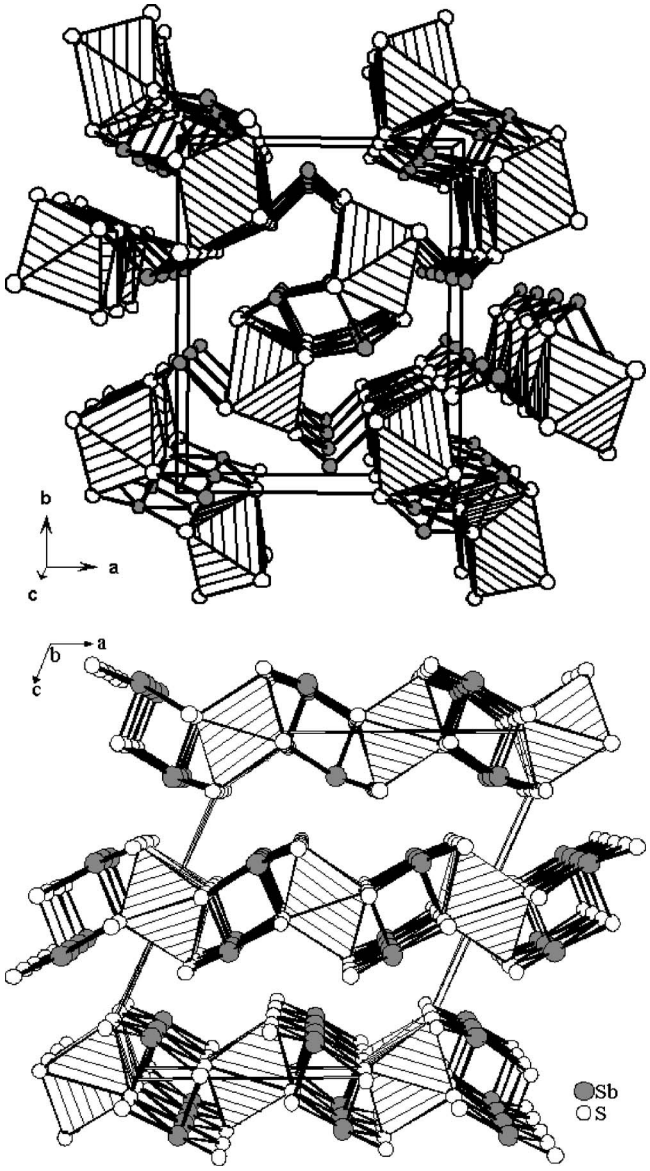


FIG. 1. Crystal structures of (a) orthorhombic and (b) monoclinic $MnSb_2S_4$. View along the chains of edge sharing $MnS_6$ octahedra, S atoms are white, Sb gray. Bonds between Sb and S are drawn only for $d(\mathrm{Sb—S}) < 3.15$ Å.

tropy imposed by the $[SbS_3]^{3-}$ units. They result in tetragonally distorted $MnS_6$ octahedra with a coordination number of 2+4 in (*mC28*) $MnSb_2S_4$ and a coordination number of 1+1+2+2 in (*oP28*) $MnSb_2S_4$, respectively. Further details are provided in Refs. 17 and 19.

Considering the magnetic coupling of manganese in the two polymorphs of $MnSb_2S_4$ the structural anisotropy provided by the $MnS_6$ chains has to be kept in mind. Thus only two contacts $d(\mathrm{Mn—Mn}) \approx 3.8$ Å are present in the title compound, and all other distances between Mn atoms are larger than 6 Å. This situation is quite different from the isotropic Mn sublattices of, e.g., $\alpha$-MnS [$12 \times d(\mathrm{Mn—Mn}) \approx 3.7$ Å] and $MnS_2$ [$12 \times d(\mathrm{Mn—Mn}) \approx 4.3$ Å]. This allows one to investigate FM models with equal Mn spin directions and AFM models with alternating Mn spins along the chains in $MnSb_2S_4$.

## III. COMPUTATIONAL FRAMEWORK

The electronic properties have been self-consistently calculated in the framework of the density functional theory (DFT)[25,26] using the ASW method as implemented by Williams *et al.*[27] and Eyert.[28] The effects of exchange and correlation were parameterized according to the local spin density approximation (LSDA) scheme of Vosko, Wilk, and Nusair.[29] All valence electrons, including $4d$(Sb) ones, were treated as band states. In the minimum ASW basis set, we chose the outermost shells to represent the valence states and the matrix elements were constructed using partial waves up to $l_{\max}=2$ quantum number. The ASW method uses the atomic sphere approximation (ASA) which assumes overlapping spheres centered on the atomic sites where the potential has a spherical symmetry. In order to represent the correct shape of the crystal potential in the large voids of the respective crystal structures, additional augmentation spheres were inserted[28] to avoid an otherwise too large overlap between the actual atomic spheres.

The calculations implicit of zero entropy ($T=0$ K) were started assuming a nonmagnetic configuration which is nonspin polarized (NSP) meaning that spin degeneracy was enforced for all species (atoms and empty spheres). Note that this configuration does not translate a paramagnetic state which would actually require a supercell with different orientations of the spins over the crystal sites. In a second step spin polarized (SP) calculations were performed by initially allowing for differing spin occupations, i.e., majority (spin up $\uparrow$) and minority (spin down $\downarrow$) spins for all atomic species. The occupancies were self-consistently changed until convergence of the total energy ($\Delta E \leqslant 10^{-6}$ Ry) and of the charges ($\Delta Q \leqslant 10^{-6}$) between two subsequent iterations was reached. For that a sufficiently large number of $k$ points was used with respect to self-consistancy of the results. In view of the large cells especially when symmetry is broken by introducing the antiferromagnetic orderings, we used up to $12 \times 12 \times 12$, i.e., 1728, points to produce, respectively, 216 and 468 $k$ points in the irreducible wedges of the orthorhombic and monoclinic Brillouin zones. Calculations are implicit of collinear magnetic structures. However, noncollinear magnetic structures can occur in manganese based compounds such as in the nitride $Mn_4N$ which was studied in the same calculational framework.[30] In fact such heavy calculations could be achieved with great accuracy in energy differences between the magnetic configurations provided one considers high symmetry structures such as that of cubic antiperovskite $Mn_4N$. When one magnetic/crystallographic sublattice of all species is accounted for, a ferromagnetic order (FM) is described. Two magnetic sublattices need to be accounted for to calculate the AFM configurations. This can be achieved by symmetry breaking of the system, half of the constituents being "spin up" and the other half being "spin down." This approach accounts for the effect of low spin and high spin $Mn^{2+}$ and spin spin interactions in AFM and FM models for $MnSb_2S_4$ similar to the incommensurate magnetic structure of $FeSb_2S_4$.[18] Indeed, spin reorientation, spin disorder, and the competition between AFM and FM orientation are discussed to play an important role in magnetic systems. We are

aware of the fact that our models do not simulate spin dynamics. However, any spin interaction as, for example, in the incommensurate AFM structure of $FeSb_2S_4$ has to be expected between the states given by the AFM, FM, and NM models. Considering the orthorhombic structure which has four $MnSb_2S_4$ formula units, two AFM configurations were accounted for, i.e., with the spin aligned oppositely in $MnS_6$ octahedral chains, this will be called hereafter AFM1 and another one with spins aligned parallel within a chain and oppositely between chains (AFM2). As for the monoclinic variety, the unit cell has two different manganese sites Mn1 and Mn2. This leads to a first possibility which is to account for antiparallel spin alignment between Mn1 and Mn2 sites leading to a ferrimagnetic (FIM) order. The other possibility is to double the cell along the third lattice vector *c* with Mn1 and Mn2 all up-↑ in the first cell and Mn1 and Mn2 all down-↓ in second cell, i.e., conforming with the spin spiral found for $MnSb_2S_4$ (*mC28*).[31] Needless to say, the symmetry breaking due to the magnetic lattice orderings among Mn(↑) and Mn(↓) in both structures' computations are much heavier to carry out, hence the limitation in the Brillouin zone integration in *k* points presented above.

Further information about the nature of the interaction between atomic constituents can be provided using overlap population (OP) leading to the so- called COOP (crystal orbital overlap population)[32] or alternatively introducing the Hamiltonian based population COHP (crystal orbital Hamiltonian population).[33] Both approaches lead to a qualitative description of the chemical interactions between two atomic species by assigning a bonding, nonbonding, or antibonding character. A slight refinement of the COHP was recently proposed in the form of the "covalent bond energy" $E_{COV}$ which combines both COHP and COOP so as to make the resulting quantity independent of the choice of the zero of potential.[34] The $E_{COV}$ was recently implemented within the ASW method.[35] Our experience with both COOP and $E_{COV}$ shows that they give similar general trends although COOP exaggerates the magnitude of antibonding states. We shall be using the $E_{COV}$ description of the chemical bonding.

## IV. CALCULATION RESULTS AND DISCUSSION

### A. Total energy and magnetic moments

Charge transfer is observed from Mn towards Sb, S and the empty spheres; nonetheless its amount is not significant in terms of an ionic description (such as $Mn^{2+}$), which is rarely observed in the framework of such calculations. A more meaningful picture is provided from the quantum mixing of the valence states as it will be shown in the plots of the density of states (DOS) and the chemical bonding ($E_{COV}$) in the next sections. The two polymorphs show similar trends concerning the total energy calculated for the nonmagnetic (NM) and spin polarized (SP) ferromagnetic (FM) and antiferromagnetic (AFM) models. Further ferrimagnetic calculations in the monoclinic system were carried out. This is detailed in Table I which presents the results obtained after self-consistent computations for the different magnetic configurations considered. For both modifications the FM state is favored with respect to the nonmagnetic one. The large gain in energy arises from the magnetic exchange of coupled high spin $Mn^{2+}$ when spin polarization is accounted for. In FM configuration the resulting total magnetization per formula unit is close to 5 $\mu_B$. For formally $Mn^{2+}$ two configurations are possible for the spin arrangements within the octahedral field of sulphur: A high spin (HS) configuration $t_{2g}^3$, $e_g^2$ with five unpaired spins and a low spin (LS) one: $t_{2g}^5$, $e_g^0$ resulting in only one unpaired spin. From this it can be suggested that at least in the ferromagnetic state divalent manganese is HS. However, the total magnetization arises from all constituents of the lattice (Table I) with the main contribution due to manganese. The SP-FM Mn moment amounts to 4.38 $\mu_B$ within (*oP28*) $MnSb_2S_4$ and 4.23 $\mu_B$ for (*mC28*) $MnSb_2S_4$. This agrees with the value calculated for $Mn^{2+}$ in MnTe (Ref. 21) and lies in the range of further LSDA results on high spin $Mn^{2+}$ from 4.3 to 4.6 $\mu_B$.[21–23] When the ferrimagnetic configuration is accounted for within the monoclinic variety a further stabilization is obtained and there is a cancelling out between moments so that total magnetization is zero. The AFM configurations show a further energy lowering for both varieties with a smaller energy difference in the orthorhombic structure. This would suggest a lower Néel temperature for the high pressure orthorhombic variety. Within this structure the AFM1 configuration with the spins aligned oppositely in $MnS_6$ octahedral chains is found to be favored with respect to the AFM2 one (i.e., with spins aligned parallel within a chain and oppositely between chains). The small lowering in the moment carried by $Mn^{2+}$ (4.34 $\mu_B$) agrees with the value observed for $\alpha$-MnS (4.1 $\mu_B$).[22] For $MnSb_2S_4$ (*mC28*) we find the same order of energies. Thus the applied method predicts the preference of an antiparallel coupling of the spins of Mn-*d* electrons in a high spin state against a parallel coupling. The close magnitudes of the moments between the FM and the AFM configurations lead to propose that the magnetic order might be Heisenberg-like whereby the magnetic susceptibility should obey a Bonner-Fischer behavior[36] which is characteristic for linear spin chains.

### B. Nonspin polarized calculation DOS and chemical bonding

The suggested NSP situation for $MnSb_2S_4$ (*oP28*) and (*mC28*) results in a metallic behavior, analogous to studies on MnS and $MnS_2$.[20–22] The site projected DOS are shown in Figs. 2(a) and 2(b). The highest occupied states cross the Fermi level $E_F$ at a high density of states which is attributed to $t_{2g}$ states from a crystal field analysis of Mn *d* states projections given in Fig. 2(c). These $Mn^{2+}$ $t_{2g}$ states are only partly occupied by five electrons. The next bands above $E_F$ are formed by the Mn $e_g$ states [Fig. 2(c)]. The splitting of the $e_g$ states results from deviations of the $MnS_6$ groups from octahedral symmetry. Antimony and sulphur *p*-states form broad bonding states with the metal states in the energy range [−6,−1 eV] (see next paragraph). The DOS at low energies are *s*-bands of Sb (−10 eV) and S (−15 eV); the latter are found at lower energy due to the higher electronegativity of sulphur as compared to antimony.

The chemical bonding within both orthorhombic and monoclinic $MnSb_2S_4$ are examined in the framework of the

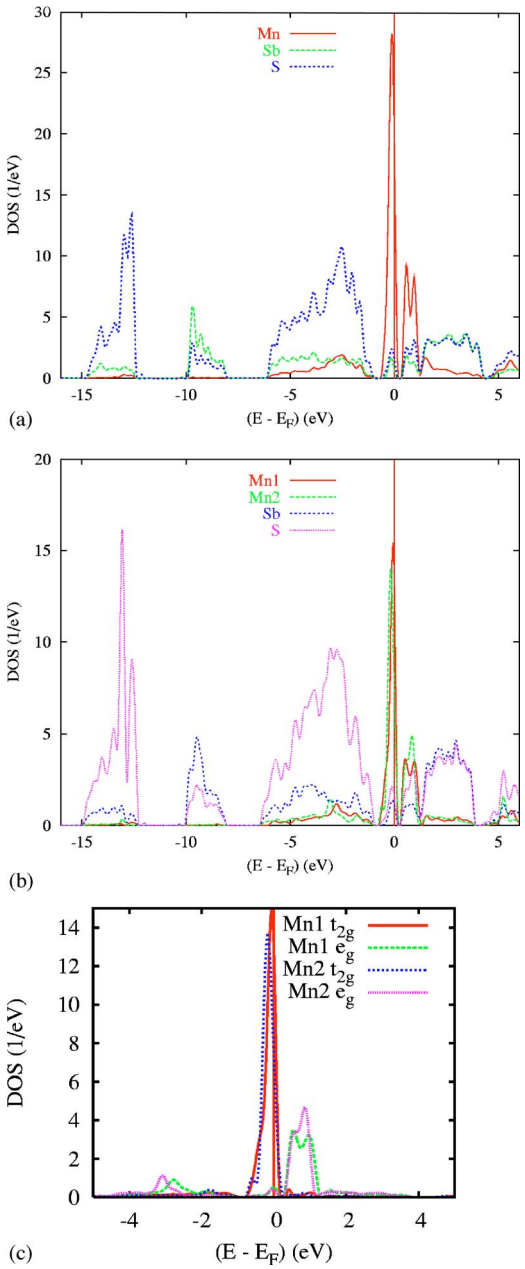


FIG. 2. (Color online) (a) and (b) Site projected DOS for one formula unit of nonmagnetic $MnSb_2S_4$ (respetively *oP28* and *mC28*). (c) $O_h$ crystal field splitting of Mn1 and Mn2 sites in $MnSb_2S_4$ (*mC28*).

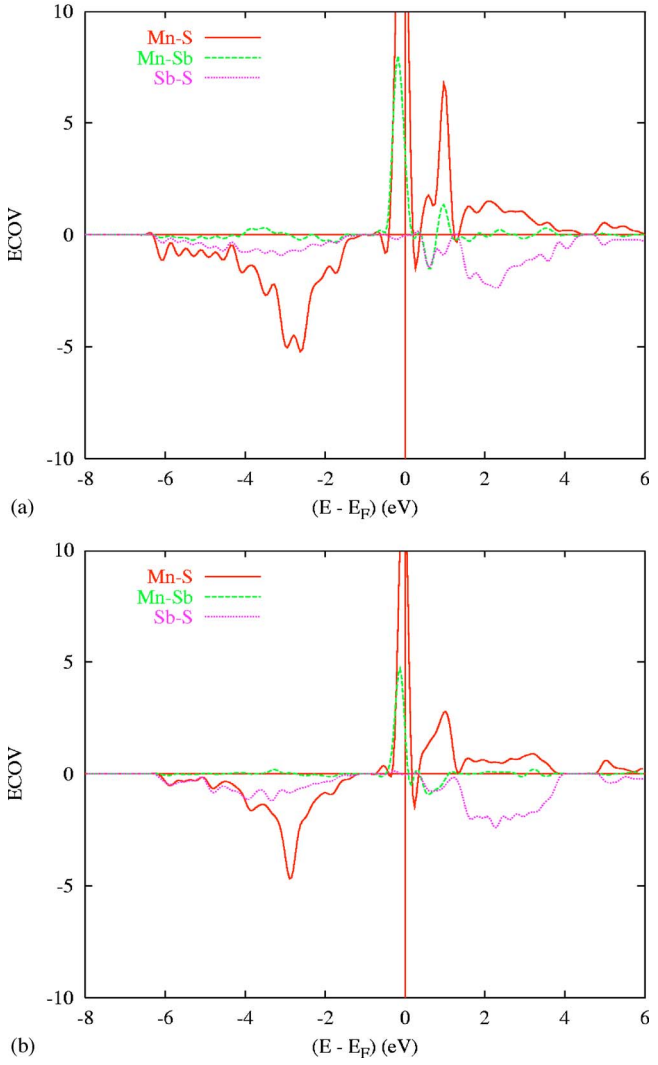


FIG. 3. (Color online) Chemical bonding properties from covalent bond energy $E_{COV}$ approach within $MnSb_2S_4$ per formula unit: (a) *oP28* orthorhombic variety and (b) *mC28* monoclinic variety for one of the two manganese sites, Sb and S regroup partial contributions from all lattice sites.

$E_{COV}$[34,35] for Mn—S, Mn—Sb, and Sb—S pair interactions. The corresponding covalent bond energy $E_{COV}$ plots are given in Figs. 3(a) and 3(b). Negative, positive, and nil $E_{COV}$ magnitudes are relevant to bonding, antibonding, and nonbonding characteristics. From this the major part of the valence band VB is bonding due to Mn—S interactions as well as to Sb—S albeit with a smaller magnitude; this contributes to the stabilization of the crystal lattice. The Sb—S interaction is observed with smaller magnitude and it remains bonding within the conduction band above $E_F$. This somehow provides an illustration for the description of the bonding given in the crystal structure section above. Mn—Sb interaction plays little role—as with respect to the Mn—S one—within the major range of the VB. At the top of the VB the system becomes largely destabilized as the Fermi level is reached, i.e., where a large Mn—S $E_{COV}$ as well as Mn—Sb antibonding interactions with smaller magnitude can be observed. Although a large part of the Mn($t_{2g}$) are not engaged into Mn—S antibonding interaction in as far as they are responsible for the onset of the Mn magnetic moment, the nonmagnetic configuration is clearly not favored from that. Lastly Mn—Mn interactions were observed too but with much smaller magnitudes than all other explicited ones in both crystal varieties, so they are not shown here. Nevertheless it will be discussed below that these bonds can have consequences on the electronic structure (cf. Sec. III C particularly for the monoclinic band structures).

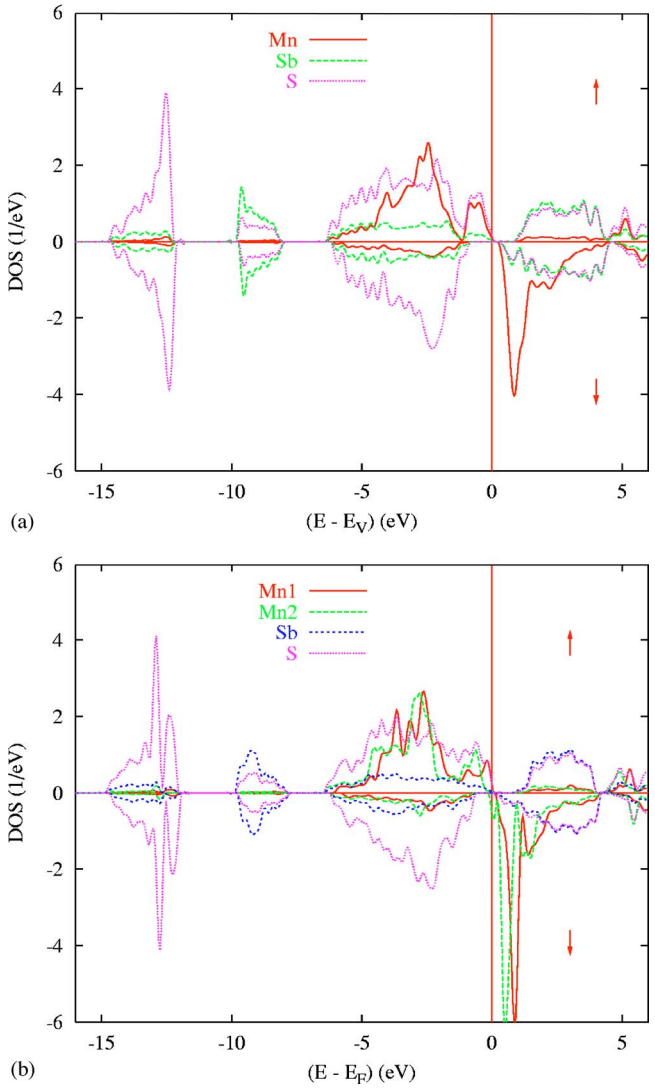


FIG. 4. (Color online) Spin resolved site projected DOS per formula unit for (a) $MnSb_2S_4$ (*oP28*) and (b) $MnSb_2S_4$ (*mC28*), Sb and S regroup partial contributions from all lattice sites.

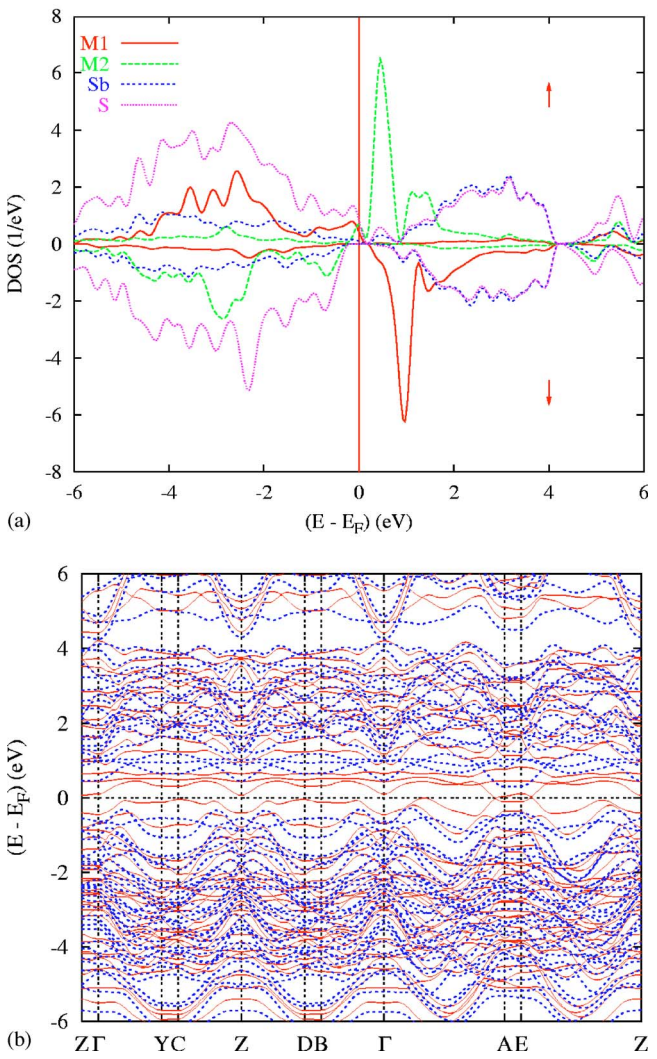


FIG. 5. (Color online) (a) DOS (M1 and M2 stand for Mn1 and Mn2, respectively; Sb and S regroup partial contributions from all lattice sites) and (b) band structure in a narrow energy window around the Fermi level of ferrimagnetic intermediate state of monoclinic $MnSb_2S_4$ (*mC28*) [solid lines (↑), dotted lines (↓)].

### C. Electronic structure of spin polarized $MnSb_2S_4$

#### *1. Ferromagnetic state*

As shown by the site projected DOS in Figs. 4(a) and 4(b), the spin polarization causes Mn 3*d* levels to split into majority spin (↑) states which are lowered in energy relative to minority spin (↓) states at higher energy. Majority Mn *d* spin states completely lie below $E_F$, thus being fully occupied by five electrons. The minority Mn *d* states are found above $E_F$ thus being completely empty. This indicates a closely nonmetallic situation with a small energy gap in the orthorhombic variety which reduces to a closing in (*mC28*) $MnSb_2S_4$. The DOS for manganese in both varieties exhibit peaks which closely resemble the $t_{2g}(\uparrow)$-$e_g(\uparrow)$ manifolds. Thus the highest occupied states in the valence band are formed by Mn up spin $e_g$ states and the lowest unoccupied ones by down spin $t_{2g}$ states. Concerning Sb and S DOS the latter can be observed to closely follow the shape of Mn pointing to the Mn—S coordination, i.e., with $MnS_6$ octahedra within which the major part of the bonding within the lattice occurs as discussed above. Spin polarization mainly affects Mn states so that there is hardly any energy shift between (↑) and (↓) spin populations for Sb and S although residual moments were computed in both orthorhombic and monoclinic systems (Table I).

#### *2. Ferrimagnetic (FIM) model in* $MnSb_2S_4$ *(mC28)*

A first possibility to account for antiparallel spin alignment within (*mC28*) $MnSb_2S_4$ was to allow for it between the two singly occupied Mn sublattices within the base centered monoclinic structure. The resulting energy differences shown in Table I are found in favor of this FIM configuration by 13.3 meV with respect to FM. The magnitudes of the moments are within range of FM calculations but the resulting magnetization is zero. The DOS and band structure are given in Figs. 5(a) and 5(b), respectively. The DOS plot shows some similar features to FM [Fig. 4(b)] but there is

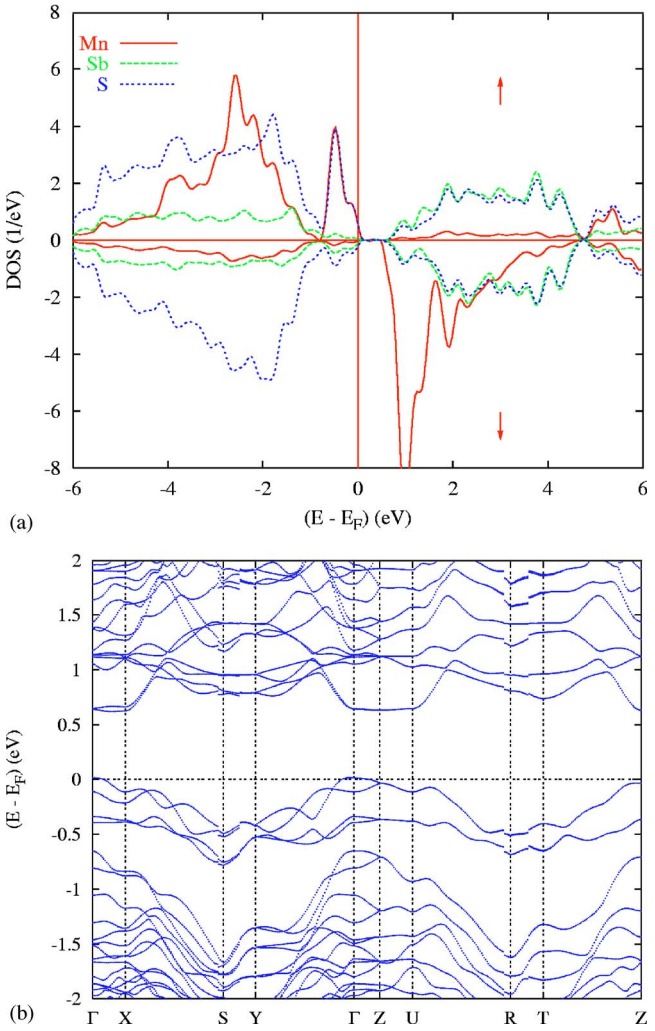


FIG. 6. (Color online) DOS and band structure in a narrow energy window around $E_F$ of antiferromagnetic ground state of orthorhombic $MnSb_2S_4$ (*oP28*).

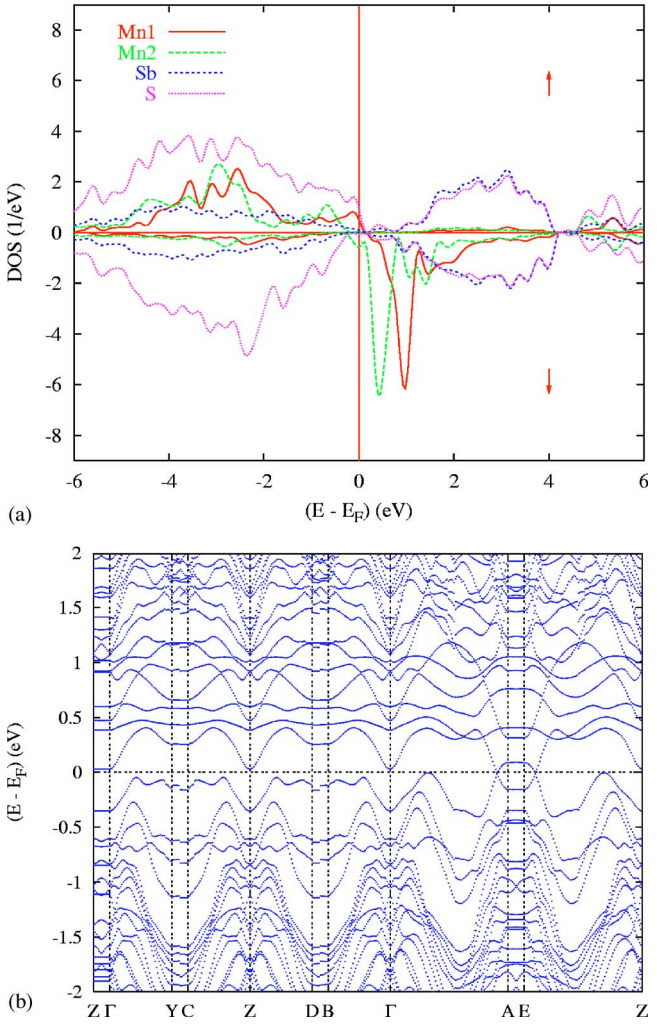


FIG. 7. (Color online) DOS and band structure in a narrow energy window around $E_F$ of antiferromagnetic ground state of monoclinic $MnSb_2S_4$ (*mC28*).

now a gap opening in the minority spins whereas a metallic behavior is observed for majority spins. From the band structure plot in the same energy window the gap of ~0.6 eV can be observed between the VB and the CB in the U(A-E) direction which is along the $k_z$ axis of the monoclinic Brillouin zone. It is along this direction that the metallic behavior is obtained too as resulting from the crossing of single bands from the VB and the CB due to a large dispersion. Thus the monoclinic system, in an intermediate magnetic state (see relative energies in Table I), is not a semiconductor but a half-metallic ferrimagnet with a relatively low DOS at $E_F$ due to single band crossing.

### *3. Antiferromagnetic (AFM) models*

For all systems the energy differences shown in Table I are in favor of AFM ground state configurations (AFM1 for *oP28*). The result of enforced AF configuration is that the total up spin and down spin projected densities of states present the same contributions. As a consequence plots for one magnetic sublattice within each structure will be shown. In a narrow energy window around the Fermi level meant to exhibit the relevant features of the AFM ground state, Figs. 6 and 7 give the DOS and band structure for orthorhombic and monoclinic AFM $MnSb_2S_4$, respectively. The $MnSb_2S_4$ (*oP28*) projected DOS (Fig. 6) show a larger splitting around $E_F$ than in the FM DOS [Fig. 4(a)]. The larger gap is likely to arise from a shift of unoccupied minority Mn states to higher energies within the CB which can be a result of Mn—Mn interactions throughout the $MnS_6$ chains. From Fig. 6(b) showing the band structure its magnitude amounts to ~0.7 eV between $\Gamma_{VB}$ and $\Gamma_{CB}$, for instance, in the orthorhombic Brillouin zone. This results in a nonconducting state. Note that this gap for the AFM state is close to the experimental value of 0.77 eV found for monoclinic system.[20] Our calculations indicate the preference of an AFM configuration (AFM1, cf. energy differences in Table I) based on a simple model of alternating Mn moments along the rods. This is somehow similar to the $\alpha$-MnS case examined by Tappero *et al.*[23]

AFM ground state site projected DOS of $MnSb_2S_4$ (*mc28*) (Fig. 7) show different features from the ferrimagnetic case

[Fig. 5(a)] because both Mn1 and Mn2 are now polarized up or down within a magnetic sublattice (see, for instance, the change of orientation of Mn1 and Mn2 DOS above $E_F$); this results in larger $n(E_F)$. In terms of band structure [Fig. 7(b)] this involves enhanced band crossing along the AE direction (along the $k_z$ direction) as it can be observed from the confrontation with the ferrimagnetic band structure [Fig. 5(b)]. From such a band dispersion and crossing the system is obtained as weakly metallic. This is somehow opposed to the semiconducting state proposed experimentally. Nevertheless both monoclinic and orthorhombic varieties have been shown to possess similar features and the final answer on the question for the coupling of the magnetic moments will be given by neutron diffraction. Related investigations are in progress.[31]

## V. CONCLUSION

The electronic structure of $MnSb_2S_4$ in both the orthorhombic and the monoclinic modifications were calculated within the local spin approximation for nonmagnetic as well as for spin polarized ferromagnetic, ferrimagnetic, and antiferromagnetic models. According to total energy calculations the spin polarized states with high spin $Mn^{2+}$ are largely preferred to a nonspin polarized one (Table I). Magnetic moments of $\sim 4.3\ \mu_B$ are calculated in agreement with high spin $Mn^{2+}$ configuration known from MnS and $MnS_2$. For both $MnSb_2S_4$ varieties the AFM model shows an additional energy gain, thus becoming the ground state. These results are accompanied by significant differences in the electronic structures of the models. The NSP model leads to a metallic behavior for both modifications with a partly filled VB formed by Mn $t_{2g}$ and the CB by the empty Mn $e_g$ bands shown by a crystal field analysis. In the orthorhombic system FM and AFM models lead to the experimentally observed semiconducting characteristics with a larger gap obtained for the AFM ground state. Differences in the electronic structures concerning the CB and the VB are due to the crystal structures. Calculations for $MnSb_2S_4$ (*oP28*) reveal a band gap of 0.7 eV, close to the experimental value of 0.77 eV. In $MnSb_2S_4$ (*mC28*) two Mn sites are present which have a significantly different environment by sulphur and therefore the site projected DOS for Mn shows a broadening, hence the VB is broadened too in comparison to the orthorhombic modification. On the other hand, the empty minority spin Mn *d* states in the conduction band are sharper for the monoclinic modification. This is related to the higher local symmetry at the Mn sites. The computed intermediate ferrimagnetic state exhibits a half metallic behavior due to single Mn bands crossing along the AE direction in the Brillouin zone, i.e., along $k_z$. This is enhanced in the AFM ground state. Although the antiferromagnetic nature of the ground state of both modifications of $MnSb_2S_4$ becomes evident by the present calculations, further investigations of electrical conductivity to reveal the semiconducting properties are needed, they are underway.

## ACKNOWLEDGMENTS

Computational facilities were provided within the intensive numerical simulation facilities network M3PEC of the University Bordeaux 1, partly financed by the *Conseil Régional d'Aquitaine*. Support from the Deutsche Forschungsgemeinschaft (DFG) through Sonderforschungsbereich 484 is equally acknowledged.

*Corresponding author. Electronic address: matar@icmcb-bordeaux.cnrs.fr

[1] P. P. Ewald and W. Friedrich, Ann. Phys. (Paris) **44**, 1183 (1914).
[2] H. Ott, Z. Kristallogr. **63**, 222 (1926).
[3] L. M. Corliss, N. Elliott, and J. Hastings, Phys. Rev. **104**, 924 (1956).
[4] G. Wistrand, Ph.D. thesis, Univ. Uppsala, Sweden, 1916. E. Wedekind, Angew. Chem. **37**, 87 (1924); W. Hofmann, Z. Kristallogr. **86**, 225 (1933).
[5] H. Haraldsen and W. Klemm, Z. Anorg. Allg. Chem. **220**, 183 (1934).
[6] S. Jin, Science **264**, 413 (1994).
[7] H. Ohno, D. Chiba, F. Matsukura, T. Omiya, E. Abe, T. Dietl, Y. Ohno, and K. Ohtani, Nature (London) **408**, 944 (2000).
[8] V. Poltavets, K. Vidyasagar, and M. Jansen, J. Solid State Chem. **177**, 1285 (2004).
[9] S. F. Matar, Solid State Sci. **4**, 1265 (2002).
[10] N. A. Spaldin and W. E. Pickett, Solid State Chem. **176**, 615 (2003).
[11] S. F. Matar, Prog. Solid State Chem. **31**, 239 (2004).
[12] E. A. Axtell III, J. Hanko, J. A. Cowen, and M. G. Kanatzidis, Chem. Mater. **13**, 2850 (2001); Z. S. Gönen, J. C. Fettinger, and B. Eichhorn, J. Solid State Chem. **155**, 305 (2000).
[13] Y. Kamihara, Y. Takeshita, M. Matoba, T. Kyomen, and M. Itoh, Nippon Oyo Jiki Gakk. **28**, 347 (2004).
[14] S. S. Aplesnin, G. A. Petrakovskii, L. I. Ryabinkina, G. M. Abramova, N. I. Kiselev, and O. B. Romanova, Solid State Commun. **129**, 195 (2004).
[15] P. Léone, L.-M. Le Leuch, P. Palvadeau, P. Molinie, and Y. Moëlo, Solid State Sci. **5**, 771 (2003).
[16] V. Tsurkan, M. Mucksch, V. Fritsch, J. Hemberger, M. Klemm, S. Klimm, S. Korner, H.-A. Krug von Nidda, D. Samusi, E.-W. Scheidt, A. Loidl, S. Horn, and R. Tidecks, Phys. Rev. B **68**, 134434 (2003).
[17] A. Bente and K. Edenharter, Z. Kristallogr. **186**, 31 (1989).
[18] M. Wintenberger and G. André, Physica B **162**, 5 (1990).
[19] A. Pfitzner and D. Kurowski, Z. Kristallogr. **215**, 373 (2000).
[20] D. Kurowski, Ph.D. thesis, University of Regensburg, 2003.
[21] S-H. Wei and A. Zunger, Phys. Rev. B **48**, 6111 (1993).
[22] D. Hobbs and J. Hafner, J. Phys.: Condens. Matter **11**, 8197 (1999); A. Rohrbach, J. Hafner, and G. Kresse, *ibid.* **15**, 979 (2003).
[23] R. Tappero, P. Wolfers, and A. Lichanot, Chem. Phys. Lett. **335**, 449 (2001).
[24] A. Kyono, M. Kimata, M. Matsuhisa, Y. Miyashita, and K. Okamoto, Phys. Chem. Miner. **29**, 254 (2002).

[25] P. Hohenberg and W. Kohn, Phys. Rev. **136**, B864 (1964).
[26] W. Kohn and L. J. Sham, Phys. Rev. **140**, A1133 (1965).
[27] A. R. Williams, J. Kübler, and C. D. Gelatt, Jr., Phys. Rev. B **19**, 6094 (1979).
[28] V. Eyert, Int. J. Quantum Chem. **77**, 1007 (2000).
[29] S. H. Vosko, L. Wilk, and M. Nusair, Can. J. Phys. **58**, 1200 (1980).
[30] M. Uhl, S. F. Matar, and P. Mohn, Phys. Rev. B **55**, 2995 (1997).
[31] D. Kurowski, A. Pfitzner, W. Kockelmann, M. H. Möller, and R. Pöttgen (unpublished).
[32] R. Hoffmann, Angew. Chem., Int. Ed. Engl. **26**, 846 (1987).
[33] R. Dronskowski and P. E. Blöchl, J. Phys. Chem. **97**, 8617 (1993).
[34] G. Bester and M. Fähnle, J. Phys.: Condens. Matter **13**, 11541 (2001).
[35] V. Eyert and S. F. Matar (unpublished).
[36] Jill C. Bonner and Michael E. Fisher, Phys. Rev. **135**, A640 (1964).